

Modeling evaporation of Jet A, JP-7 and RP-1 drops at 1 to 15 bars

Kenneth Harstad, Josette Bellan *

4800 Oak Grove Drive, M/S 125-109, Jet Propulsion Laboratory, California

Institute of Technology, Pasadena, California 91109-8099

Abstract

A model describing the evaporation of an isolated drop of a multicomponent fuel containing hundreds of species has been developed. The model is based on Continuous Thermodynamics concepts wherein the composition of a fuel is statistically described using a Probability Distribution Function (PDF). Following previous studies, this PDF is parametrized on the species molar weight. However, unlike in previous studies, a unified formulation is developed wherein the same PDF holds for three major homologous hydrocarbon classes. The new PDF is a double-Gamma-PDF that is parametrized on the square root of the molar weight. The additional advantage of the formulation is that it is valid in the subcritical region from 1 to 15 bars. Discrete species distributions for Jet A, JP-7 and RP-1 are fitted using this novel PDF and extensive calculations for isolated drops of these kerosenes are performed. The results show that under the quasi-steady gas phase assumption, the D^2 law is recovered after an initial transient. The evaporation constant is (1)

an increasing function of of the far field temperature and pressure, (2) a complex function of far field composition according to the values of the far field temperature and pressure, and (3) a strong function of the far field pressure but a weak function of the difference between the surface and far field vapor molar fraction. The composition of the vapor at the drop surface is kerosene-fuel specific. A comparison between results obtained with a model assuming the drop interior to be well mixed and a model wherein the drop may evaporate either in a well-mixed mode or at unchanging composition shows that the percentage difference between the evaporation constant predicted by the two models is within the range of uncertainty in the transport properties.

Key words: Evaporation of multi-component drops

1 Introduction

Kerosene has been used as aviation fuel ever since the advent of the jet-engine aircraft. In the gas turbine engines powering aircraft, kerosene is injected through an atomizer whose role is to produce a fine spray. The drops evaporate, thereby providing the vapor which burns and powers the aircraft. The purpose of atomization is to increase the area of the liquid, and thus to facilitate evaporation. Tailoring of the atomization processes for better (i.e.

* Corresponding Author

Email address: Josette.Bellan@jpl.nasa.gov, Tel: (818) 354-6959, Fax: (818) 393-5011 (Josette Bellan).

improved combustion) drop size distribution crucially depends on the understanding of drop evaporation under a wide range of far field conditions.

Kerosene is a nomenclature that encompasses fuels that are complex mixtures of species, each mixture containing hundreds of components [1]. Such fuels are JP-4, JP-5, JP-7, JP-8, Jet A and RP-1. Fuels that are mixtures of many chemical species are called “multi-component” (MC) to differentiate them from fuels that are composed of a single chemical species (SC). Although the importance of understanding the evaporation of MC fuels has been recognized more than thirty years ago, it is not until recently that it has been addressed in its full MC complexity. Early studies focussing on very detailed models of binary species drops [2]-[7] yielded valuable information regarding the intricacies of internal drop processes. However, this detailed model was not intended for utilization in spray calculations. Abramzon and Sirignano [8] used the understanding thus derived to propose an internal drop model that is one dimensional but embeds the more complex behavior of multidimensionality. The full MC aspect of liquid drop composition has been much less addressed. An early example of full MC drop model is that of Law and Law [9] who assumed that the evaporation rate was much faster than the time for change of the internal drop composition, and thus that the drop was basically evaporating at fixed composition. Further work by Makino and Law [10] showed that the regime of fixed-composition evaporation (which is liquid-phase diffusion-limited) prevails when the drop Peclet number Pe based on the asymptotic

(i.e. after the drop transient have relaxed) evaporation rate is large, whereas for small values of this number, the evaporation is distillation-like and changes the approximately-uniform composition of the mixture inside the drop as a function of time. In all these models, the mixture composition was considered as a discrete sum of all the chemical species.

More recently, the limit of the well-mixed, distillation-like evaporation has been modeled in a statistical manner by Tamim and Hallett [11] and Hallett [12] by using Continuous Thermodynamics (CT) concepts. CT is a theory (see [13]-[17]) in which the composition of a mixture is described by a probability distribution function (PDF) rather than by a series of discrete values of the concentration. Generally, this PDF depends on all thermophysical properties of the chemical species, however, in practical applications it can be chosen to depend on one or several properties of interest of the mixture [16] such as the relative volatility [13], the normal boiling point, the number of carbon atoms per molecule, or the molar weight [17]. The simplification that the PDF depends only on the molar weight is possible for mixtures composed of homologous species [17] [19] and such homologous-class-specific distributions, based on the Gamma PDF (Γ -PDF), have been proposed for diesel fuel, gasoline and kerosene [11] [17]. Whitson [18] used the Γ -PDF

$$f_{\Gamma}(m) = \frac{(m - \gamma)^{\alpha-1}}{\beta^{\alpha}\Gamma(\alpha)} \exp\left[-\left(\frac{m - \gamma}{\beta}\right)\right] \quad (1)$$

to characterize the high molar-weight portion of crude oils, where m is the

molar weight and $\Gamma(\alpha)$ is the Gamma function. The origin of f is specified by γ , and its shape is determined by parameters, α and β ; α, β and γ are related to the mean, θ , the variance, σ^2 , and the second moment, ψ , of f by $\theta = \alpha\beta + \gamma$, $\sigma^2 = \alpha\beta^2$, $\psi = \theta^2 + \sigma^2$. Thus, the advantage of CT theory is that the mixture composition can be represented by a small number of parameters rather than by the very large number of parameters necessary for a discretely described fuel. The theory is based on the appropriate representation of the chemical potential for a mixture containing numerous components and uses molecular thermodynamic methods to represent the Gibbs function in terms of this PDF. The concepts are fundamental and independent of the physicochemical model chosen to represent the chemical potential. For a specified initial PDF, the evolution of the mixture is governed by thermodynamic relationships and/or conservation equations. The CT method has been successfully used for (i) calculating vapor-liquid equilibrium [11] [20], (ii) computing liquid-liquid equilibrium [20], (iii) simulating polymer solutions [17] [20] [18], (iv) computations of distillation [20], (v) flash calculations [17] [18] [21], (vi) characterization of carbon plus fractions [18] and (vii) modeling MC-fuel drop evaporation [11] [23].

The single- Γ -PDF model described by Tamim and Hallett [11] and Hallett [12], was found by Lippert [22] and Lippert and Reitz [23] to be a good representation for drop evaporation only when the far field contains a small amount of fuel vapor. Indeed, the single- Γ -PDF inherently cannot accommodate con-

condensation onto the drop that may create a second peak in the mixture distribution. This limitation was quantified by Harstad et al. [24] who derived a more general model, based on two superimposed Γ -PDFs, called the double- Γ -PDF, which can accommodate a wide range of drop far field conditions. Thus, the double- Γ -PDF is

$$P_l(m; \alpha_1, \beta_1, \alpha_2, \beta_2, \varepsilon) = (1 - \varepsilon)f_\Gamma^{(1)}(m) + \varepsilon f_\Gamma^{(2)}(m), \quad (2)$$

where $f_\Gamma^{(q)}(m) = f_\Gamma(m; \alpha_q, \beta_q)$ with $q \in [1, 2]$, ε is a weighting parameter ($0 \leq \varepsilon \leq 1$) and $\int_\gamma^\infty P_l(m)dm = 1$. To determine P_l as a function of time, one needs to solve for the vector $\eta \equiv (\alpha_1, \beta_1, \alpha_2, \beta_2, \varepsilon)$ at each time step. A method for obtaining this vector has been developed [24] and the accuracy of the double- Γ -PDF model to portray a discrete distribution was verified by comparing its predictions with statistics from a discrete species model.

Another limitation of CT theory with the PDF of eqs. 1 and 2 is that when the PDF depends on m , the Γ -PDF representation is homologous species dependent, meaning that the parameters α , β and γ of $f_\Gamma^{(q)}(m)$ may change with the class of hydrocarbons. This increases the complexity of a fuel representation because it is necessary to have a double- Γ -PDF for each homologous class entering the fuel composition. Since for each homologous class one would need to solve for the vector $\eta \equiv (\alpha_1, \beta_1, \alpha_2, \beta_2, \varepsilon)$ at each time step, it is clear that the computation would become very cumbersome, negating the advantages of the CT formulation.

One novelty of the formulation presented below is that a method was found to characterize the behavior of individual hydrocarbon classes to allow the utilization of the same Gamma PDF to describe three homologous classes that are the principal contributors to of kerosenes; these classes are alkanes, naphthenes and aromatics [1]. With this new formulation, the advantage of the CT representation is maintained. Another novelty of the present formulation is that it is valid in the subcritical regime for pressures up to 15 bars, in contrast to all existing CT models which hold only at atmospheric pressure. The increased validity of the model at larger than atmospheric pressure is an important aspect in the context of its applicability for gas turbine engine applications.

This paper is organized as follows: We first describe the thermodynamics and transport properties of hydrocarbon classes which allows the 1-15 bars pressure representation of the three homologous classes (using the same Γ -PDF function) that are the main constituents of kerosenes. With this new representation, the Γ -PDF becomes a function of $m^{0.5}$ rather than m [11] [12] [18] [22] [23] [24]. Then, we briefly recall the double- Γ -PDF model of Harstad et al. [24] in the context of the new $m^{0.5}$ dependency of the Γ -PDF. Results are presented for three kerosenes, whose composition, provided by Edwards [25] as a discrete bar chart, was fitted to portray a double- Γ -PDF. Using the well-mixed model, a detailed parametric study is conducted for Jet A as a function of the far field conditions. Further, the results from the well-mixed model are

compared with those from a model wherein the criterion of $Pe = 1$ decides whether the drop evaporates in the well-mixed composition mode ($Pe < 1$) or the frozen-composition mode ($Pe \geq 1$). To determine the effect of the fuel initial composition, calculations are also performed with RP-1 and JP-7 for different far field conditions. Finally, we summarize the results and present conclusions.

2 Model equations

2.1 Thermodynamics and transport properties of hydrocarbon classes

The driving idea behind the correlations presented below is the derivation of a unified thermodynamic representation for the three homologous classes of interest as functions of judiciously chosen functions. Indeed, once the drop composition is known, Raoult's law in continuous form is used to relate the vapor PDF at the drop surface, $P_v^{(s)}$, to the known $P_l^{(s)}$ and the surface vapor mole fraction $X_v^{(s)}$ through

$$P_v^{(s)} = \frac{p_{sat}(T, \mu)}{X_v^{(s)} p^{(\infty)}} P_l^{(s)} \quad (3)$$

as shown in [24], where μ is the distribution variable and $p^{(\infty)}$ is the far field pressure. This means that to unify the representation of homologous class properties, attention should be focussed on modeling p_{sat} in a general manner that is simple enough to be functionally usable and that also introduces the

needed dependency on μ . We consider here isomers frequently used in fuel surrogates [1], namely n-alkanes (heptane through hexadecane), cyclopentane, cyclohexane, methylcyclohexane, benzene, toluene, m-xylene, butylbenzene and 1-methylnaphthalene.

The intent is to characterize hydrocarbons in each series or class by m , as well as by unified reference quantities that depend on m and thermodynamic quantities. The point of departure is the saturation curve $p_{sat}(T)$ for each hydrocarbon, whose inverse is $T_{sat}(p)$. For a specified hydrocarbon, and thus given m , this curve defines a one-to-one mapping between T and p , and this mapping is approximated by a fit which maps the reference temperature T_{ref} to the reference pressure p_{ref} as

$$T_{ref} = T_{bn}/[1 - 0.127 \ln(p_{ref}/p_{atm})/m^{0.066}] \quad (4)$$

where T_{bn} is the saturation (i.e. boiling point) temperature in degrees K at $p_{atm} = 1.01325$ bar and m is in g/mol. Equation 4 is not used as a functional form representation of the actual saturation curve; it only represents a point mapping between T_{ref} and p_{ref} . In fact, the saturation curve is given by a modeled relationship that fits the desired unified form. This modeled relationship is found by considering the function $A_s(p_{ref}) \equiv [d(\ln p_{sat})/d(\ln T)]_{T=T_{ref}}$ which is fitted for $p_{ref} \lesssim 15$ bars as

$$A_s(p_{ref}) = 6.95 m^{0.10} (p_{atm}/p_{ref})^{0.135} \quad (5)$$

with an error of 1.5% or less. Then, a hydrocarbon saturation curve may be

expressed by

$$p_{sat}(T, m) = w_s(T) p_{ref} \exp[A_s(1 - T_{ref}/T)] \quad (6)$$

where by comparison with $p_{sat}(T)$, one finds $w_s(T_{ref}) \doteq 1$ and $[dw_s/dT]_{T_{ref}} \doteq 0$. This means that eq. 6 with w_s set to unity is asymptotically exact near T_{ref} because T_{ref} is near the saturation temperature T_{sat} at p_{ref} .

Another thermodynamic quantity of interest is the latent heat, $L_v(T)$ which is related to the saturation pressure p_{sat} through the Clausius-Clapeyron relation

$$L_v(T) = \frac{R_u T^2}{m} \frac{d \ln(p_{sat})}{dT} \Delta Z_v, \quad (7)$$

where R_u is the universal gas constant, $Z = p/(\rho T R_u/m)$ is the compression factor portraying departures from the perfect gas behavior (i.e. $Z = 1$) and $\Delta Z_v \equiv Z_v - Z_l$ expresses the change in Z during evaporation. Within the new model developed here

$$L_v(T_{ref}, p_{ref}, m) = A_s \Delta Z_v (R_u T_{ref}/m). \quad (8)$$

For $p_{ref} \lesssim 15$ bar, curve fits of the NIST SuperTRAPP data [26] give

$$\Delta Z_v = 1 - a_d m^{0.60} (p_{ref}/p_{atm})^{0.75} \text{ and } Z_v = 1 - a_z m^{0.60} (p_{ref}/p_{atm})^{0.70} \quad (9)$$

where constants a_d and a_z for the three hydrocarbon series are given in Table 1. Furthermore, if one defines $A_{bn} \equiv T_{bn}/m^{0.5}$, it is clear from its values listed in Table 1 that A_{bn} is nearly constant for each hydrocarbon series. Errors in ΔZ_v and Z_v values are $\leq 1\%$, except at the highest pressures (i.e. $\simeq 12 - 15$

bars), where errors of $O(5\%)$ may occur. At any specified p_{ref} , constants a_d , a_z and A_{bn} define the saturation behavior of a hydrocarbon series through T_{ref} given by eq. 4 and L_v given by eqs. 8 and 9. The variation of a_d , a_z and A_{bn} between series is relatively weak (see Table 1), hence the behavior of a kerosene mixture is assumed to be that of a single series with constants calculated as volume weighted averages of the component series constants. Based on series weights for Jet A, JP-7 and RP-1 [1], constants for these fuels are given in Table 1.

To completely unify the hydrocarbon class representation, a model is needed for the saturation vapor thermal conductivity, λ_v , the isobaric heat capacity, C_v , the saturation liquid heat capacity C_l , and the liquid density, ρ_l . Denoting any of these four properties by Λ , for a hydrocarbon series, their temperature dependence may be represented for 10^{-2} bars $\lesssim p_{sat} \lesssim 15$ bars as

$$\Lambda(T) = \Lambda_{bn} f_{\Lambda}(T/T_{bn}) \quad (10)$$

where $0.7 \lesssim T/T_{bn} \leq 1.35$ and Λ_{bn} is the property value at T_{bn} (i.e. $f_{\Lambda}(1) = 1$) whose dependency on m is given in Table 1. For λ_v , C_v , C_l and ρ_l , the NIST code SuperTRAPP [26] was used to generate the data that allowed the fits. For completeness, the density at the critical point, ρ_c , is also listed. Plots of f_{Λ} are given in Figs. 1a-1d. The same figures contain fits representing mean functions that are used with kerosene models; the mean values Λ_{bn} are given in Table 1 for Jet A, JP-7 and RP-1. These mean functions are given as cubic

polynomials in the Appendix. Function deviations are largest at the highest T (i.e. at highest saturation pressure), being there 3% – 5%. For all fuels, $\rho_l \simeq 0.8 \text{ g/cm}^3$ at $T = 60 \text{ F}$, in agreement with the values listed in [1]. At 15 bars, which is the largest pressure considered, the minimum ρ_l (i.e. at T_{sat}) is $\rho_l \simeq 0.5 \text{ g/cm}^3$ (see Table 1 and Fig. 1d), thus justifying the classical quasi-steady (with respect to the liquid phase) gas-phase assumption.

2.2 Drop model

The variation of p_{sat} with m , as given by eq. 6 with T_{ref} given by eq. 4 where $T_{bn} \propto m^{0.5}$, suggests that the Γ -PDF should no longer be function of m , but instead should be function of $m^{0.5}$. This conclusion is reinforced by the dependency of the kerosene fuel properties with m , as listed in Table 1. Therefore, we use here the model developed by Harstad et al. [24], but with a new dependency of the Γ -PDF

$$f_{\Gamma}^*(m) = \frac{(m^{0.5} - \gamma^*)^{\alpha^* - 1}}{\beta^* \alpha^* \Gamma(\alpha^*)} \exp \left[- \left(\frac{m^{0.5} - \gamma^*}{\beta^*} \right) \right] \quad (11)$$

and

$$P_l^*(m; \alpha_1^*, \beta_1^*, \alpha_2^*, \beta_2^*, \varepsilon) = (1 - \varepsilon) f_{\Gamma}^{*(1)}(m) + \varepsilon f_{\Gamma}^{*(2)}(m), \quad (12)$$

where $f_{\Gamma}^{*(q)}(m) = f_{\Gamma}^*(m; \alpha_q^*, \beta_q^*)$ with $q \in [1, 2]$, ε is a weighting parameter ($0 \leq \varepsilon \leq 1$) and $\int_{\gamma^*}^{\infty} P_l^*(m) d(m^{0.5}) = 1$. Reference quantities used to unify the

fuel class representation are

$$T_{ref} = m^{0.5} A_{bn} / [1 - 0.127 \ln(p_{ref}/p_{atm}) / m_{ref}^{0.066}], \quad (13)$$

$$m_{ref} = \xi_{11} m_s^{0.5}, \quad m_s^{0.5} \simeq (T_d/A_{bn}) - 0.127 \ln(p_{ref}/p_{atm}) (T_d/A_{bn})^{0.868} \quad (14)$$

where m_s is the molar weight value at $T_{ref} = T_d$, where T_d is the drop temperature and

$$\xi_{nl} \equiv \int_{\gamma^*}^{\infty} m^{0.5n} P_l^*(m) d(m^{0.5}) = \langle\langle m^{0.5n} \rangle\rangle \text{ for } n \geq 1 \quad (15)$$

$$\xi_{nv} \equiv \int_{\gamma^*}^{\infty} m^{0.5n} P_v^*(m) d(m^{0.5}) = \langle m^{0.5n} \rangle \text{ for } n \geq 1 \quad (16)$$

are the moments of P_l^* and P_v^* ; $\langle\langle \rangle\rangle$ and $\langle \rangle$ denote the expectations over P_l^* and P_v^* , respectively. By definition, $P_v(m) = P_v^*(m)/(2m^{0.5})$ and $P_l(m) = P_l^*(m)/(2m^{0.5})$. The value of m_{ref} is also used in the functions A_s , ΔZ_v and Z_v . The advantage of this new representation is that the distribution function P_l^* is valid over the three homologous hydrocarbon series examined, instead of needing a class-dependent distribution function.

With the new dependency on the distribution variable, the model derived by Harstad et al. [24] can still be applied. This model calculates for specified gas far field ($p^{(\infty)}$, temperature $T^{(\infty)}$ and vapor molar fraction $X_v^{(\infty)}$) and drop initial conditions (initial size D_0 , initial temperature T_{d0} and composition given by a single- or double- Γ -PDF) a solution represented by T_d , the drop diameter, D , and the drop internal composition. The vapor composition at the drop surface is calculated using boundary conditions; here the unified form of

Raoult's law is used with p_{sat} in eq. 3 given by eq. 6 with unity w_s . The vapor distribution between the drop surface and the gas far field is calculated utilizing the classical quasi-steady assumption which allows the finding of an analytic gas phase solution.

The crucial part in obtaining the solution is based on finding P_l^* . This is theoretically accomplished by solving equations for the first five moments of P_l^* , at each time step, which provide the information to solve for the vector $\eta^* \equiv (\alpha_1^*, \beta_1^*, \alpha_2^*, \beta_2^*, \varepsilon)$ that determines P_l^* . The moment equations are CT forms of those derived from statistics of a discrete molar weight liquid-distribution [24] and are

$$\frac{d\xi_{nl}}{dt} = \frac{3\rho_g^{(s)}\mathcal{D}_{eff}m_l}{\rho_l R^2 m_g^{(s)}} \frac{1+B_m}{B_m} \ln(1+B_m) \times \quad (17)$$

$$\left[\left(X_v^{(s)} - X_v^{(\infty)} \frac{1-X_v^{(s)}}{1-X_v^{(\infty)}} \right) \xi_{nl} - \left(X_v^{(s)} \xi_{nv}^{(s)} - X_v^{(\infty)} \frac{1-X_v^{(s)}}{1-X_v^{(\infty)}} \xi_{nv}^{(\infty)} \right) \right],$$

where t is the time, $\rho_g^{(s)}$ is the gas density at the drop surface (superscript s), \mathcal{D}_{eff} is an effective gas diffusion coefficient, $m_l = \xi_{2l}$, R is the drop radius, $m_g = m_{ag}(1 - X_v) + \xi_{2v}X_v$ where m_{ag} is the molar weight of air, and $B_m \equiv (Y_v^{(s)} - Y_v^{(\infty)})/(1 - Y_v^{(s)})$. Consistently, $\rho_g = \rho_v X_v + \rho_{ag}(1 - X_v)$ with $\rho_v = pm_v/(Z_v R_u T)$ and $\rho_{ag} = pm_{ag}/(Z_{ag} R_u T)$ where $Z_{ag} = 1$.

Equation 17 is the CT form of the discrete species equation inside the drop and embeds information from the solution of the quasi-steady differential equations in the gas phase to which boundary conditions at the drop surface and far field have been applied. The cumbersome mathematics of solving for η^*

from the knowledge of the five moments [24], would however negate the computationally efficient aspect of the model; moreover, the liquid composition may not entirely follow the double- Γ -PDF functional relationship, which is only an approximation of the real distribution. Therefore, in practice only four moments are used; one of the five components of η^* is determined from an empirical formula derived from a thorough analysis of combinations of the moments.

Classical equations, recast in the present formulation, are solved for D and T_d

$$\frac{dD^2}{dt} = -\frac{8\rho_g^{(s)}\mathcal{D}_{eff}}{\rho_l} \ln(1 + B_m), \quad (18)$$

$$\frac{dT_d}{dt} = \frac{3\lambda_g^{(s)}}{\rho_l C_l R^2} \left[(T^{(\infty)} - T_d) \frac{\ln(1 + B_T)}{B_T} - \frac{L_v^* \ln(1 + B_m)}{C_p^* Le B_m} \right] \quad (19)$$

where $(1 + B_T) \equiv (1 + B_m)^{1/Le}$, the Lewis number is $Le \equiv \lambda_g^{(s)} / (C_p^* \rho_g^{(s)} \mathcal{D}_{eff})$

and

$$L_v^* = L_v^{(s)}(1 + B_m) - L_v^{(\infty)}, \quad L_v^{(s)} = Y_v^{(s)} < L_v >^{(s)}, \quad L_v^{(\infty)} = Y_v^{(\infty)} < L_v >^{(\infty)} \quad (20)$$

$$C_p^* = Y_v^{(s)} C_v^{(s)} + (1 - Y_v^{(s)}) [C_{ag} + (C_v^{(s)} - C_{ag}) B_m / \ln(1 + B_m)] \quad (21)$$

$$< L_v >^{(s)} = \frac{R_u T_{bn}}{\xi_{2v}^{(s)}} A_s(p^{(\infty)}, m_{ref}) \frac{1 - a_d m_{ref}^{0.60} (p^{(\infty)} / p_{atm})^{0.75}}{1 - 0.127 \ln(p^{(\infty)} / p_{atm}) / m_{ref}^{0.066}} \quad (22)$$

where $T_{bn} = A_{bn} < m^{0.5} >^{(s)}$, m_{ref} is given by eq. 14 with $p_{ref} = p^{(\infty)}$, and

$C_{ag} = R_u \tilde{\gamma} / [(\tilde{\gamma} - 1) m_{ag}]$ where $\tilde{\gamma}$ is the perfect gas constant. Consistently, all

(gas) transport properties are calculated at the drop surface, as in Miller et

al. [27].

3 Results

Following a preliminary discussion of the initial conditions, results are presented encompassing a wide range of far field conditions. All calculations were performed for $D_0 = 1$ mm and $T_{d0} = 300$ K, as the focus of this study is on liquid composition and evolving gas composition during evaporation rather than other drop parameters. The results first emphasize the behavior of Jet A (because among the three kerosenes it is the fuel with the most complex form of the $m^{0.5}$ distribution; see below) under a wide range of conditions, particularly as a function of pressure; these results are obtained with the well-mixed (wm) model described above. To inquire how these results depend on the model, calculations are then performed with another model in which the Makino and Law [10] criterion on Pe is utilized to switch the computation between the two limiting cases of well-mixed and frozen composition (fc) models; this combined model is denoted by “wm-fc”. In the frozen drop-composition model, $d\xi_{nl}/dt = 0$, and P_l^* does not change with t . As mentioned in the Introduction, in [10], the criterion on Pe is based on an asymptotic evaporation rate constant, $K^{(a)}$, which is unknown before the calculation is performed; therefore, this criterion is here applied with the instantaneous rather than asymptotic Pe . Comparisons of results obtained with the wm-fc model are then compared to those obtained with the wm model. Finally, the effect of fuel composition is studied with the wm model, because this model allows the evolution of the mixture composition during evaporation. In sprays, rela-

tively cold drops may initially be exposed to relatively high gas temperatures, and thus evaporate in a fc limit mode as soon as the drop temperature has risen enough to render the evaporation rate larger than the diffusional process rate inside the drop. However, as fuel vapor accumulates in the gas, the drop evaporation rate may decrease and thus evaporation may occur in the wm regime; this situation will certainly prevail in dense portions of sprays where coking and sooting occur. Among all models based on average properties in the drop, only the wm model can account for mixture composition changes and the accompanying vapor composition variations during evaporation.

The equations are solved using a 4th order Fehlberg Runge-Kutta method with variable step size and the relative error tolerance was 10^{-5} .

3.1 Initial and far field conditions

The mole fraction distribution as a function of molar weight was provided to us [25] for Jet A, JP-7 and RP-1 in the form of bar charts. Complementary information was also provided [25] in the form of tables for each one of these three fuels describing its composition in terms of the carbon number. As stated above, alkanes, naphthenes and aromatics were preponderant in the composition [1]. The information thus available was fitted to the distribution of eq. 12 for each of the three kerosene fuels, leading to the parameters of Table 2. Noteworthy, only Jet A has a truly double- Γ -PDF composition; JP-7 fits eq.

11, while RP-1 is intermediary between Jet A and JP-7. Also, for the three fuels, the minimum molar weight of the species entering the composition is the same: $(\gamma^*)^2 = 93$ g/mol. The mean molar weight of all fuels is similar, with JP-7 and RP-1 being very close. The standard deviation of Jet A is noticeably larger than that of JP-7 or RP-1, for which it is almost the same. The three distributions are illustrated in Fig. 2, where both the raw data (denoted “input”) and the fits are displayed. The fits appear to be very good considering the typical uncertainty in the data.

The far field conditions used in the calculations are listed in Table 3 for Jet A and Table 4 for JP-7 and RP-1. To calculate $\langle L_v \rangle^{(\infty)}$, $\xi_{nv}^{(s)}$ at $t = 0$ is used for the value of $\xi_{nv}^{(\infty)}$, and $[\xi_{1v}^{(\infty)}]^2$ is taken to be m_{ref} .

3.2 Drop evaporation

3.2.1 Parametric study for Jet A

Displayed in Fig. 3a -3c are the D^2/D_0^2 , T_d and $T_d / \langle \langle T_{sat} \rangle \rangle$ temporal variations for $p^{(\infty)} = 1$ (3a and 3b) and 10 (3a and 3c) bars at several $T^{(\infty)}$. Clearly, the D^2 law is obeyed after the initial drop-heating transient, independent of $p^{(\infty)}$ and $T^{(\infty)}$. With increasing $p^{(\infty)}$, the drop heat-up time increases (Fig. 3a), independent of $T^{(\infty)}$, as observed under microgravity conditions by Nomura et al. [28] for heptane drops in nitrogen. Examination of Fig. 3a also shows that at low $T^{(\infty)}$ the drop lifetime, t_{life} , increases with in-

creasing $p^{(\infty)}$, whereas at high $T^{(\infty)}$ the opposite happens; at an intermediary $T^{(\infty)}$, t_{life} seems independent of $p^{(\infty)}$. Depicted in Fig. 3d is t_{life} versus $T^{(\infty)}$ at $X_v^{(\infty)} = 0$ for several $p^{(\infty)}$; the drop lifetime was obtained as the intersect of the D^2/D_0^2 curve with the t/D_0^2 axis. The plot is directly comparable with Fig. 8 of Nomura et al. [28]. Similar to Nomura's results for heptane drops in nitrogen, we find that for Jet A drops in air there is a pivot in $T^{(\infty)}$ separating a low $T^{(\infty)}$ region where t_{life} increases with increasing $p^{(\infty)}$ from a high $T^{(\infty)}$ region where the opposite behavior with $p^{(\infty)}$ is encountered. Therefore, we conclude that Nomura's results [28] are also valid for MC drops.

Unlike for SC drops, T_d for Jet A (Figs. 3b and 3c) continues to increase during the drop lifetime independent of $p^{(\infty)}$ and $T^{(\infty)}$; this increase is explained by the fact that the saturation temperature continuously increases with the drop composition as the volatile species preferentially evaporate. At higher $p^{(\infty)}$ the heating rate is larger and drops attain larger temperatures. Figures 3b and 3c show that indeed T_d quickly reaches values close to $\ll T_{sat} \gg$ and asymptotically tends to it at the end of the drop lifetime. As the drops become minute, numerical artifacts unphysically increase T_d and produce a kink in $T_d/\ll T_{sat} \gg$; however, the fate of the drops is no longer of interest at that point.

To examine the evolutions of the surface-vapor mean molar weight $\xi_{2v}^{(s)}$ and the weight standard deviation derived from P_v^* , $\sigma_v^{(s)} \equiv [\xi_{4v}^{(s)} - (\xi_{2v}^{(s)})^2]^{0.5}$, plots are presented in Figs. 4a ($p^{(\infty)} = 1$ bar) and 4b ($p^{(\infty)} = 10$ bars) at three values of

$T^{(\infty)}$; for evaluation purposes they are compared at $p^{(\infty)} = 1$ bar and $T^{(\infty)} = 600$ K to results from a discrete species model based on 20 components [24]. The surface-vapor mean molar weight continuously increases with time as the volatile species preferentially evaporate from the drop, however, the rate of $\xi_{2v}^{(s)}$ increase is larger with increasing $T^{(\infty)}$ and decreasing $p^{(\infty)}$, which is attributed to the larger T_d versus t/D_0^2 when $T^{(\infty)}$ increases at specified $p^{(\infty)}$ (Figs. 3b and 3c). For the smaller $T^{(\infty)}$ values, the rate of $\xi_{2v}^{(s)}$ increase is larger with decreasing $p^{(\infty)}$, which is attributed to a larger $T_d/ \ll T_{sat} \gg$ when $p^{(\infty)}$ decreases at specified $T^{(\infty)}$ (Figs. 3b and 3c); at $T^{(\infty)} = 1000$ K, the same trend can be seen during most of the drop lifetime in terms of residual mass, M_d/M_{d0} , but as the drop becomes small, the trend slightly reverses. The evolution of $\sigma_v^{(s)}$ displays a non-monotonic timewise variation, independent of the far field conditions. An initial surge corresponds to that of $T_d/ \ll T_{sat} \gg$ and is due to the rapid drop heat up which continuously removes the most volatile species from the drop: as T_d increases, higher m components are evaporated, which increases $\sigma_v^{(s)}$. As $T_d/ \ll T_{sat} \gg$ asymptotes, so does $\sigma_v^{(s)}$ since the differential distillation diminishes. The $T_d/ \ll T_{sat} \gg$ asymptotic value reached is smaller than unity, increases with $T^{(\infty)}$ and decreases with $p^{(\infty)}$. The double- Γ -PDF based on $m^{0.5}$ captures excellently the discrete predictions. In Fig. 4a, the discrete model results are not shown as they entirely coincide with those of the double- Γ -PDF; in Fig. 4b, a slight deviation of the double- Γ -PDF from the discrete model occurs over a negligible m range and is due

to the inherent approximations involved in the mathematical solution of the moment equations. To further characterize the molar weight distribution at the drop surface, ε is illustrated in Fig. 4c. It is clear that the tendency for the P_l^* and P_v^* distributions is to become single- Γ -PDFs as the drop evaporates. At larger $T^{(\infty)}$ or smaller $p^{(\infty)}$, the rate of evolution towards a single- Γ -PDF is higher, with the dependency on $T^{(\infty)}$ being much stronger than on $p^{(\infty)}$. Finally, $P_v^{(s)}(m)$ is displayed in Fig. 5 versus m at two different stages of the drop life, 60% (Fig. 5a) and 20% (Fig. 5b) residual mass, at $p^{(\infty)} = 1, 5, 10$ and 15 bars at $T^{(\infty)} = 1000$ K. At 60% residual mass, all distributions except that at 1 bar are similar, indicating that for relatively short evaporation times the evolution of the distribution is a weak function of $p^{(\infty)}$. However, slightly broader distributions and with a smaller mean molar weight are obtained at the larger that atmospheric $p^{(\infty)}$, consistent with the previous result showing that $\xi_{2v}^{(s)}$ decreases with $p^{(\infty)}$. At 20% residual mass, $P_v^{(s)}(m)$ exhibits more differentiation as a function of $p^{(\infty)}$, displaying a shift of its peak to lower values and a decreased mean molar weight with larger $p^{(\infty)}$.

To summarize the behavior of the drop under a variety of far field conditions, portrayed in Fig. 6a is the evaporation constant, $K \equiv -dD^2/dt$ in the asymptotic D^2 law regime as a function of $p^{(\infty)}$ at three values of $T^{(\infty)}$ and two values of $X_v^{(\infty)}$. Note that K is not indicative of the drop lifetime as it does not account for the heat up time which increases with increasing $p^{(\infty)}$ and decreasing $T^{(\infty)}$. The results show that K is an increasing function of

$T^{(\infty)}$, $p^{(\infty)}$ and a complex function of $X_v^{(\infty)}$ according to the values of $T^{(\infty)}$ and $p^{(\infty)}$. At $p^{(\infty)} = 1$ bar, K decreases with increasing $X_v^{(\infty)}$ which is due to the decreasing evaporation rate occurring when the conditions are closer to saturation. This smaller evaporation rate at $T^{(\infty)} = 600$ K is also responsible for the decreasing K with increasing $X_v^{(\infty)}$ at all $p^{(\infty)}$. At larger $T^{(\infty)}$, a threshold is reached in $p^{(\infty)}$ beyond which at a specified $p^{(\infty)}$, K increases with increasing $X_v^{(\infty)}$; this result is not easily (cause-and-effect) explainable, as K does not necessarily portray the drop lifetime. The drop lifetime (discussed above) is the heat-up time, which indirectly depends on $X_v^{(\infty)}$, added to the evaporation time in the purely quasi-steady mode defined as the region where K is constant. The different dependence of K on $X_v^{(\infty)}$ at higher than atmospheric $p^{(\infty)}$ indicates that results from $p^{(\infty)} = 1$ bar measurements are not directly extendable to higher pressures. To further illustrate the complex dependency of the drop behavior with $X_v^{(\infty)}$, $T^{(\infty)}$ and $p^{(\infty)}$, the magnitude of the evaporation-driving molar potential, $X_v^{(s)} - X_v^{(\infty)}$, is plotted in Fig. 6b in the asymptotic D^2 law regime as a function of $p^{(\infty)}$ at different $T^{(\infty)}$ and $X_v^{(\infty)}$. Whereas $X_v^{(s)} - X_v^{(\infty)}$ slightly increases with $p^{(\infty)}$ at the larger values of $T^{(\infty)}$, at $T^{(\infty)} = 600$ K this quantity is virtually invariant with $p^{(\infty)}$; these results are independent of $X_v^{(\infty)}$. Therefore, it can be concluded that at larger $T^{(\infty)}$, K is a strong function of $p^{(\infty)}$, whereas $X_v^{(s)} - X_v^{(\infty)}$ is a weak function of $p^{(\infty)}$. The functional dependence of K on $X_v^{(s)} - X_v^{(\infty)}$ is not easily determined in the CT context.

All results discussed above were obtained with $Le = 0.5$, this value being a factor of two estimate made from the gas transport properties. Similar results obtained for $Le = 1$ (not shown) displayed the same trends.

3.2.2 Combined well-mixed and frozen-composition model

Comparisons between the wm and wm-fc models were performed to inquire about the differences between the two models. The criterion for switching between the two limiting-case models is conservative with respect to the utilization of the wm model in that it may switch the calculation to the fc model somewhat early with respect to the criterion in [10], and thus amplify differences between the wm and wm-fc models. Given eq. ??, the criterion is set as follows: if $B_m > B_m^*$, then $d\xi_{nl}/dt$ is replaced by $[\exp(1 - B_m/B_m^*)](d\xi_{nl}/dt)$, which ensures that the switch is not abrupt. The value of $B_m^* = 0.025$ ensures that the criterion is conservative ($Pe = 1$ was calculated to correspond to $B_m \cong 0.1$).

The results are depicted in Fig. 7 for Jet A. At both $p^{(\infty)} = 1$ bar (Fig. 7a) and 10 (Fig. 7b) bars, the deviations between wm and wm-fc models are very small for D^2/D_0^2 and certainly within the range of accuracy of the thermodynamic properties at all values of $X_v^{(\infty)}$, $T^{(\infty)}$ and $p^{(\infty)}$ investigated. The difference between the two models is in the prediction of T_d which continuously increases with t in the wm model whereas it asymptotes with the unchanging composition in the wm-fc model. Scrutiny of the results shows that the wm model

is quickly replaced by the fc model when $X_v^{(\infty)} = 0$; this pivot between the models occurs at no less than 99% residual mass. When $X_v^{(\infty)} = 0.3$, the wm model is followed during drop growth, whereas the fc model becomes operative as soon as net evaporation ensues; as an example, the switch happens at 1.19% and 1.48% residual mass for $p^{(\infty)} = 1$ and 10 bars, respectively.

Figure 8 shows K obtained with each of the two models for all kerosenes as a function of $p^{(\infty)}$ at $X_v^{(\infty)} = 0$ and $T^{(\infty)} = 1000$ K. Since the calculations switch from the wm to the fc model very early in the drop lifetime, K is representative of either the wm or (when the wm-fc results are considered) of the fc calculation. Clearly, the differences between predictions with the two models are more pronounced for Jet A (5% at $p^{(\infty)} = 1$ bar and 18% at $p^{(\infty)} = 15$ bars), and very small for JP-7 and RP-1. Also, the differences between models increase with pressure, this being attributed to the increase of the saturation temperature with pressure.

Since detailed MC drop models incorporating differential species diffusion inside the drop (to our knowledge, no such calculation has yet been performed that includes a very large number of species) would give results intermediary between those of the limiting-case models, it can be concluded from examination of Fig. 8 that at $p^{(\infty)} = 1$ bar the differences in the value of K due to the utilization of the simpler models is very small, and certainly comparable to uncertainties in transport properties and thermodynamics. At larger $p^{(\infty)}$ the error increases, but the % error is still very small compared to the large un-

certainties in high-pressure hydrocarbon diffusion coefficients [29] that would be involved in detailed MC drop calculations. Of course, the difference between the models is mainly in the prediction of the gas composition resulting from evaporation. For MC fuels and in sprays containing millions of drops, it is clear that only limit-case models based on drop average conditions can be considered, as even with these models the simulation CPU time is several thousand hours [30].

3.2.3 *Effect of the initial fuel composition on the surface vapor composition*

Since at specified far field conditions, the drop surface composition determines the composition in the gas surrounding the drop, $P_v^{(s)}(m)$ is plotted in Fig. 9 ($p^{(\infty)} = 1$ bar for $X_v^{(\infty)} = 0$ (Fig. 9a) and $X_v^{(\infty)} = 0.3$ (Fig. 9b)) for all kerosenes at 60% and 20% residual mass; results at higher pressures are similar (not shown). Independent of $p^{(\infty)}$, the PDFs appear single peaked when $X_v^{(\infty)} = 0$ and double peaked when $X_v^{(\infty)} = 0.3$, this being the reason that the double- Γ -PDF model was developed [24] to describe evaporation in gaseous surroundings containing vapor. Jet A PDFs have lower peaks and are wider, this being a combined manifestation of the initial conditions (Table 2) and the evaporative process, and indicates that Jet A remains more heterogeneous in composition than the other two kerosenes.

At $p^{(\infty)} = 1$ bar and $X_v^{(\infty)} = 0$, as evaporation proceeds, $P_v^{(s)}(m)$ of Jet A changes from being wider on the low m side than those for JP-7 and RP-

1, to being wider on the high m side indicating that comparatively, Jet A evaporation tends to accumulate more heavy species. At $p^{(\infty)} = 1$ bar and $X_v^{(\infty)} = 0.3$, evaporation also widens the PDF of Jet A more than that of the other two kerosenes, but additionally now there is a differentiation between JP-7 and RP-1. In comparison with JP-7, when $X_v^{(\infty)} = 0.3$, RP-1 develops a larger distribution at the low m indicating a preferential condensation of the low volatility components onto the drop. Therefore, the results indicate that the gas composition in the vicinity of evaporating drops of Jet A, JP-7 and RP-1 will have quite different composition when in a combustion chamber.

4 Summary and conclusions

A model has been developed to describe the behavior of isolated drops of kerosenes at different pressures, temperatures and composition of the surrounding gas (pure air or air and vapor). The model is based on Continuous Thermodynamic concepts wherein the composition is represented by a probability distribution function of species properties rather than by an addition of discrete species. Consistent with previous representations proposed in the literature, the PDF is here parametrized only by the molar weight. Such distributions have been shown to be a good species-homologous-class representation. By an appropriate choice of the reference values for computing transport and thermodynamic properties, the present analysis extends the PDF representa-

tion on the molar weight to be nearly homologous class independent. The first advantage of this new representation is that one PDF is representative of the entire fuel composition, rather than having a sum of PDFs, one per homologous class, as it would have been previously necessary. The second advantage of the formulation is that the compression factor, which represents departures from the perfect gas relation, is an intrinsic part of the homologous-class-independent generalization, which makes the model valid in the subcritical region up to a far field pressure of 15 bars. In this new representation, the PDF is parametrized by the square root of the molar weight, instead of the molar weight at the power unity as it was previously done.

Jet A, JP-7 and RP-1 compositions given by discrete classes of components are then fitted in the context of this new representation. For each of these three kerosenes, the result is a double- Γ -PDF. Using these PDFs as initial conditions, extensive calculations (based on a previously developed double- Γ -PDF model that assumes gas phase quasi-steadiness and a well-mixed drop interior) are presented at different far field temperatures, pressures and gas compositions. For drops in air, the drop lifetime plotted as a function of the far field temperature at different pressures is qualitatively similar to microgravity experimental results for heptane in nitrogen, showing that the experimental data trends extend to multicomponent drops.

For $X_j^{(\infty)} = 0$, following an initial heat-up time during which the drop size is approximately constant, the drops continuously decrease in size when in air.

However, when the far field gas contains vapor, the drop experiences, concomitant with heat-up, an initial growth which is due to species condensing onto the drop; eventually, a peak in drop size is reached after which the drop size decreases as net evaporation ensues. In all cases, the D^2 law is obeyed after the initial transient. The drop temperature continuously increases as the saturation temperature of the liquid changes due to the more volatile species leaving the drop; the ratio of the instantaneous by the saturation drop temperature increases sharply during the initial drop transient and eventually asymptotes to a value smaller than unity; the asymptotic value increases with the far field temperature and decreases with the far field pressure. Plots of the evaporation constant show that it is an increasing function of the far field temperature and pressure, and a complex function of far field composition according to the values of the far field temperature and pressure. The evaporation constant is shown to be a strong function of the far field pressure but the molar evaporation potential (the difference between the surface and far field vapor molar fraction) a weak function of the far field pressure.

The vapor composition at the drop surface becomes a single- Γ -PDF when the drop evaporates in air, but displays with time an increasing double- Γ -PDF aspect when the drop evaporates in a mixture of air and vapor. In the latter case, the lower molar weight peak increases with time and eventually dominates the higher molar weight one. Simulations performed for Jet A, JP-7 and RP-1 show that the gas composition evolving during evaporation is kerosene-

type specific. During evaporation in a gas containing air and fuel vapor, Jet A tends to accumulate heavier species than JP-7 or RP-1, and RP-1 develops a larger distribution at low molar weight than JP-7, indicating a preferential condensation of the low volatility components onto the drop.

Results obtained with a model wherein the drop composition was allowed to change in the well-mixed regime or be ‘frozen’ according to an adopted criterion from the literature, showed that the evaporation constant obtained in these two limit-case models is very similar. The differences at low pressure were of the order of the accuracy in the fitted properties. At higher pressures, the differences in the evaporation constant increased between the two limit-case models explored; however, large uncertainties in the high-pressure hydrocarbon diffusion coefficients [29] would impart a similar uncertainty in results that would be obtained from a detailed calculation of the drop internal processes. Such a detailed calculation has not yet been carried out for a mixture containing a large number of species, indicating that despite increasing computational capabilities, this detailed model may be considered an impractical strategy for multicomponent spray calculations.

5 Appendix

The mean functions representing fits in Figs 1a -1d are given by

$$f_{\lambda_v}(x) = -1.055 + 3.35x - 2.515x^2 + 1.22x^3$$

$$f_{C_v}(x) = -0.916 + 4.60x - 4.474x^2 + 1.79x^3$$

$$f_{C_i}(x) = -0.705 + 4.295x - 4.20x^2 + 1.61x^3$$

$$f_{\rho_i}(x) = 1.71 - 1.31x + 1.105x^2 - 0.505x^3$$

Acknowledgment

This study was conducted at the California Institute of Technology, Jet Propulsion Laboratory, and was sponsored by the Air Force Research Laboratory, Wright Patterson Air Force Base (WPAFB), through Universal Technology Corporation, with Dr. Tim Edwards of WPAFB as Program Manager.

References

- [1] T. Edwards, L. Q. Maurice, *Journal of Propulsion and Power* 17(2) (2001) 461-466.
- [2] R. B. Landis, A. F. Mills, *Fifth International Heat Transfer Conference*, Tokyo, Japan, 1974, paper B7.9.
- [3] C. K. Law, S. Prakash, W. A. Sirignano, *Sixteenth Symposium (International)*

- on Combustion, The Combustion Institute, Pittsburgh, 1977, p. 605.
- [4] P. Lara-Urbaneja, W. A. Sirignano, Eighteenth Symposium (International) on Combustion, The Combustion Institute, Pittsburgh, 1981, p. 1365.
- [5] A. Y. Tong, W. A. Sirignano, *Combust. Flame* 66 (1986) 221-235.
- [6] C. M. Megaridis, W. A. Sirignano, Twenty Third Symposium (International) on Combustion, The Combustion Institute, Pittsburgh, 1991, p. 1413
- [7] C. M. Megaridis, W. A. Sirignano, *Combust. Sci. Tech.* 87 (1992) 27-44.
- [8] B. Abramzon, W. A. Sirignano, *Int. J. Heat Mass Transfer* 32 (1989) 1605-1618.
- [9] C. K. Law, H. K. Law, *AIAA J.* 20 (1982) 522-527.
- [10] A. Makino, C. K. Law, *Combust. Flame* 73 (1988) 331-336.
- [11] J. Tamim, W. L. H. Hallett, *Chemical Engineering Science* 50(18) (1995) 2933-2942.
- [12] W. L. H. Hallett, *Combust. Flame* 121 (2000) 334-344.
- [13] J. R. Bowman, W. C. Edmister, *Ind. Che. Eng.* 43 (1951) 2625-2628.
- [14] W. C. Edmister, J. R. Bowman, *Chem. Eng. Prog. Symp. Ser.* 48 (1952) 46-51.
- [15] R. Aris, R. R. Gavalas, *Phil. Trans. R. Soc. A* 260 (1966) 351-393.
- [16] J. G. Briano, E. D. Glandt, *Fluid Phase Equilibria* 14 (1983) 91-102.
- [17] R. L. Cotterman, R. Bender, J. M. Prausnitz, *Ind. Eng. Chem. Process Des. Dev.* 24(1) (1985) 94-203.
- [18] C. H. Whitson, *Soc. Pet. Eng. J.* 23 (1983) 683-694.

- [19] B. Gal-Or, H. T. Cullinan, Jr., R. Galli, *Chem. Eng. Sci.* 30 (1975) 1085-1092.
- [20] M. T. Rätzsch, H. Kehlen, *Fluid Phase Equilibria* 14 (1983) 225-234.
- [21] G. F. Chou, J. M. Prausnitz, *Fluid Phase Equilibria* 30 (1986) 75-82.
- [22] A. M. Lippert, Modeling of multicomponent fuels with application to sprays and simulation of Diesel engine cold start, Ph. D. Thesis, 1999, University of Wisconsin, Madison.
- [23] A. M. Lippert, R. D. Reitz, (1997) SAE Paper 972882
- [24] K. G. Harstad, P. C. Le Clercq, J. Bellan, A statistical model of multicomponent-fuel drop evaporation for many-drop gas-liquid flow simulations, in revision, the *AIAA J.* 2003.
- [25] T. Edwards, private communication (2002)
- [26] NIST Standard Reference Database 4 (SuperTRAPP), NIST Thermophysical Properties of Hydrocarbon Mixtures Database: Version 3.0 beta test version; National Institute of Standards and Technology: Gaithersburg, MD, 1999.
- [27] R. S. Miller, K. Harstad, J. Bellan, *Int. J. of Multiphase Flow* 24 (1998) 1025-1055
- [28] H. Nomura, Y., Ujiie, H. S., Rath, J., Sato, M. Kono, *Proc. of the Comb. Inst.* 26 (1996)1267-1273
- [29] K. Harstad, J. Bellan, High-pressure diffusion coefficients for combustion applications, submitted for publication, 2003

[30] Okong'o, N. and Bellan, J., Consistent Large Eddy Simulation of a temporal mixing layer laden with evaporating drops. Part I: Direct Numerical Simulation and formulation, submitted J. Fluid Mech., 2002

Property	Hydrocarbon					
	n-alkane	naphthene	aromatic	Jet A	JP-7	RP-1
$a_d \times 10^3$	3.2	2.9	2.6	3.0	3.1	3.0
$a_z \times 10^3$	2.96	2.73	2.43	2.8	2.85	2.8
$A_{bn} (\text{molK/g})^{0.5}$	37.1	38 ^[+1.0;-0.5]	40 ^[+2.0;-0.5]	38	37.5	37.7
$\lambda_{vbn} (\text{W/mK}) \times 10^3$	$2.01m^{0.48}$	$0.378m^{0.84}$	$0.74m^{0.68}$	$1.138m^{0.60}$	$1.158m^{0.60}$	$0.726m^{0.70}$
$C_{vbn} (\text{J/gK})$	$0.39 m^{0.36}$	$0.07 m^{0.70}$	$0.099 m^{0.60}$	$0.186 m^{0.50}$	$0.192 m^{0.50}$	$0.116 m^{0.60}$
$C_{lbn} (\text{J/gK})$	$0.75 m^{0.26}$	$0.317 m^{0.42}$	$0.32m^{0.40}$	$0.485 m^{0.34}$	$0.485 m^{0.34}$	$0.485 m^{0.34}$
$\rho_{lbn} (\text{g/cm}^3)$	0.60	0.715	0.78	0.665	0.65	0.67
$\rho_c (\text{g/cm}^3)$	0.233	0.27	0.29	0.25	0.25	0.25

Table 1

Properties of hydrocarbon classes and kerosene fuels. Exponents in brackets denote the error range.

	Jet A	JP-7	RP-1
α_1^*	9.733	19.45	20.0
α_2^*	14.27	11.606	12.634
$\beta_1^* (\text{g/mol})^{0.5}$	0.331	0.1686	0.161
$\beta_2^* (\text{g/mol})^{0.5}$	0.1	0.1	0.1
$(\gamma^*)^2 (\text{g/mol})$	93	93	93
ϵ	0.1357	0.0	7.35×10^{-3}
$\xi_{2l} (\text{g/mol})$	161	167.5	165
$[\xi_{4l} - \xi_{2l}^2]^{0.5} (\text{g/mol})$	29.7	19.5	19.1

Table 2

Initial liquid-fuel distribution parameters.

$p^{(\infty)}$ (bar)	$X_v^{(\infty)}$	Le		$T^{(\infty)}$ (K)						
1	0	0.5	1*	600	700	800	900	1000		
5	0	0.5	1*	600	700	800	900	1000		
10	0	0.5	1*	600	700	800	900	1000		
15	0	0.5	1*	600	700	800	900	1000		
1	0.3	0.5	1*	600	-	800	-	1000		
5	0.3	0.5	1*	600	-	800	-	1000		
10	0.3	0.5	1*	600	-	800	-	1000		
15	0.3	0.5	1*	600	-	800	-	1000		

Table 3

Initial conditions for Jet-A simulations. In all runs $D_0 = 1$ mm and $T_{d,0} = 300$ K.

$Le = 1^*$ was used only in conjunction with $T^{(\infty)} = 1000$ K.

$p^{(\infty)}$ (bar)	$X_v^{(\infty)}$
1	0 or 0.3
5	0
10	0 or 0.3
15	0

Table 4

Initial conditions for JP-7 and RP-1 simulations. In all runs $D_0 = 1$ mm $T_{d,0} = 300$

K, $T^{(\infty)} = 1000$ K and $Le = 0.5$.

Figure Captions

Figure 1. Transport and thermodynamic properties of alkanes, naphthenes and aromatic chemical classes, and global fits versus T/T_{bn} . (a) $\lambda_v/\lambda_{v,bn}$, (b) $C_{pv}/C_{pv,bn}$, (c) $C_l/C_{l,bn}$ and (d) $\rho_l/\rho_{l,bn}$.

Figure 2. The PDF of kerosenes versus the carbon number; input data [25] and fits according to eq. 12. (a) Jet A, (b) JP-7 and (c) RP-1.

Figure 3. Evaporation of a Jet A drop at $X_v^{(\infty)} = 0$ for $p^{(\infty)} = 1$ and 10 bars and $T^{(\infty)} = 600$ K, 800 K and 1000 K. Timewise (i.e. t/D_0^2) evolution of (a) D^2/D_0^2 , (b) T_d (in K) and $T_d/ \ll T_{sat} \gg$ for $p^{(\infty)} = 1$ bar, (c) T_d (in K) and $T_d/ \ll T_{sat} \gg$ for $p^{(\infty)} = 10$ bars, and (d) Jet A drop lifetime (in s) as a function of $T^{(\infty)}$ at $p^{(\infty)} = 1, 5, 10$ and 15 bars and $X_v^{(\infty)} = 0$. Legend: $-\cdot-\cdot-$ $p^{(\infty)} = 1$ bar, $T^{(\infty)} = 600$ K; $-\cdot-\cdot-$ $p^{(\infty)} = 10$ bars, $T^{(\infty)} = 600$ K; $-\cdot-\cdot-$ $p^{(\infty)} = 1$ bar, $T^{(\infty)} = 800$ K; $-\cdot-\cdot-$ $p^{(\infty)} = 10$ bar, $T^{(\infty)} = 800$ K; $-\cdot-\cdot-$ $p^{(\infty)} = 1$ bar, $T^{(\infty)} = 1000$ K; $-\cdot-\cdot-$ $p^{(\infty)} = 10$ bars, $T^{(\infty)} = 1000$ K. In 3b and 3c, the circle symbol denotes the curves representing $T_d/ \ll T_{sat} \gg$.

Figure 4. Characteristics of $P_v^{(s)}$ for a Jet A evaporating drop at $X_v^{(\infty)} = 0$ for $p^{(\infty)} = 1$ and 10 bars and $T^{(\infty)} = 600$ K, 800 K and 1000 K. Timewise (i.e. t/D_0^2) evolution of (a) mean $\xi_{2v}^{(s)}$ in g/mol, (b) standard deviation $\sigma_v^{(s)} \equiv [\xi_{4v}^{(s)} - (\xi_{2v}^{(s)})^2]^{0.5}$ in g/mol and (c) ε . For 4a and 4b, the legend is the same as in Fig. 3; additionally, the discrete model results in 4b are indicated by $-\bigcirc-\cdot-\bigcirc-\cdot-$ $p^{(\infty)} = 1$ bar, $T^{(\infty)} = 600$ K.

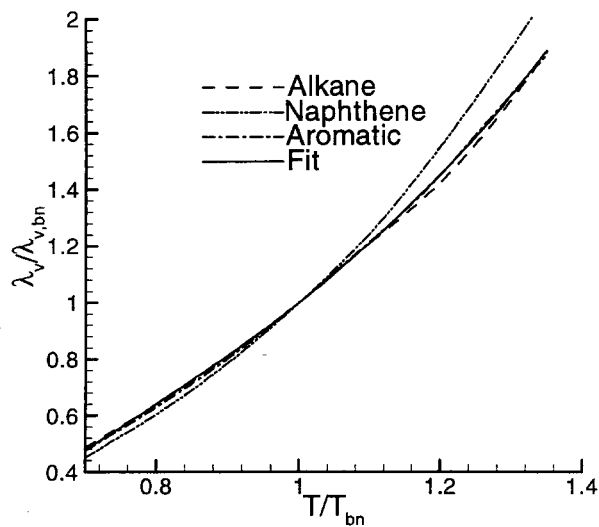
Figure 5. $P_v^{(s)}(m)$ of a Jet A evaporating drop at $X_v^{(\infty)} = 0$, for $p^{(\infty)} = 1, 5, 10$ and 15 bars and $T^{(\infty)} = 1000$ K at two stages of the drop residual mass M_d/M_{d0} (a) $M_d/M_{d0} = 0.6$, and (b) $M_d/M_{d0} = 0.2$.

Figure 6. Global evaporation characteristics versus $p^{(\infty)}$ for a Jet A drop at $X_v^{(\infty)} = 0$ and 0.3, and $T^{(\infty)} = 600$ K, 800 K and 1000 K. (a) K in mm^2/s and (b) $X_v^{(s)} - X_v^{(\infty)}$.

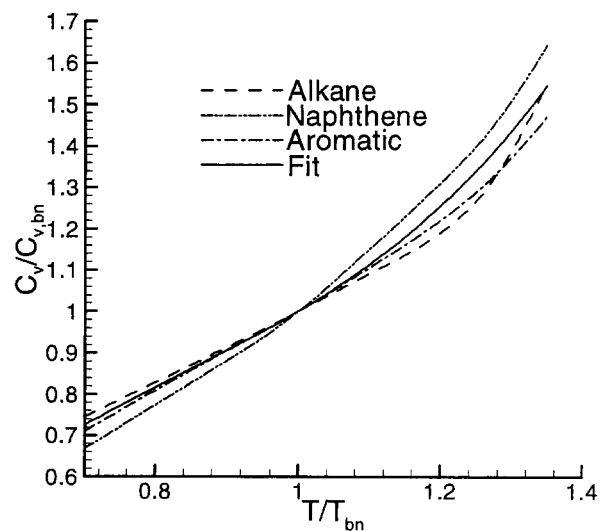
Figure 7. Comparisons between the wm and wm-fc models for an evaporating Jet A drop at $X_v^{(\infty)} = 0$ and 0.3, and $T^{(\infty)} = 1000$ K. Timewise (i.e. t/D_0^2) evolution of (a) D^2/D_0^2 and T_d (in K) at $p^{(\infty)} = 1$ bar, and (b) D^2/D_0^2 and T_d (in K) at $p^{(\infty)} = 10$ bars. The legend is: — wm model, $X_v^{(\infty)} = 0$; - - - wm model, $X_v^{(\infty)} = 0.3$; - · - wm-fc model, $X_v^{(\infty)} = 0$; - · · - wm-fc model, $X_v^{(\infty)} = 0.3$.

Figure 8. The evaporation constant K versus $p^{(\infty)}$ for all kerosenes at $X_v^{(\infty)} = 0$ and $T^{(\infty)} = 1000$ K for the wm and wm-fc models.

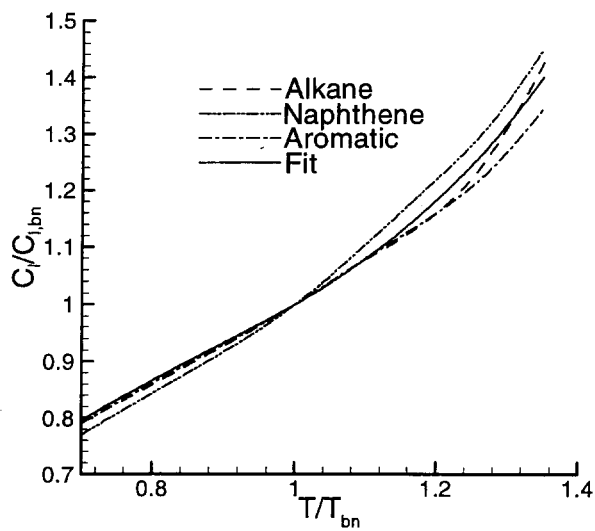
Figure 9. $P_v^{(s)}(m)$ for all kerosenes for $p^{(\infty)} = 1$ bar and $T^{(\infty)} = 1000$ K at 60% and 20% residual mass. (a) $X_v^{(\infty)} = 0$ and $X_v^{(\infty)} = 0.3$. The legend is: — Jet A, $M/M_{d0} = 0.6$; - - - Jet A, $M/M_{d0} = 0.2$; - · - JP-7, $M/M_{d0} = 0.6$; — — — JP-7, $M/M_{d0} = 0.2$; - · · - PR-1, $M/M_{d0} = 0.6$; - - - - RP-1, $M/M_{d0} = 0.2$.



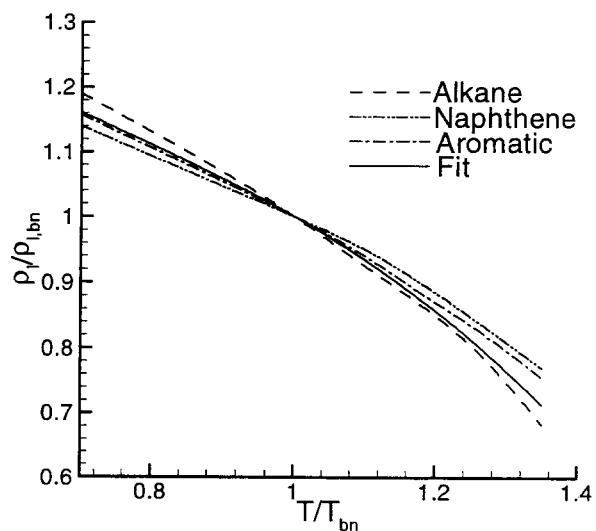
(a)



(b)

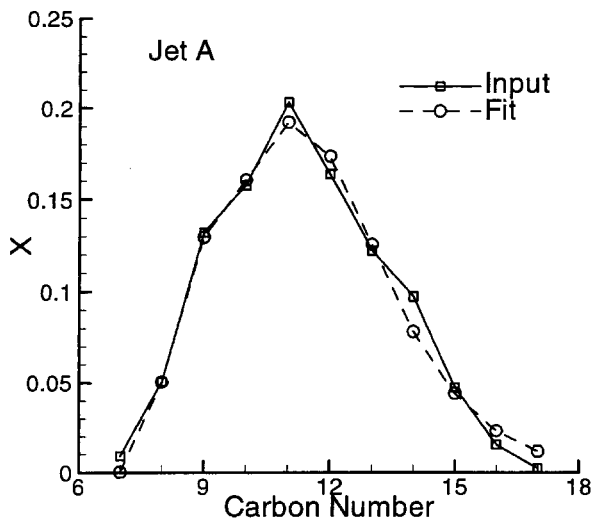


(c)

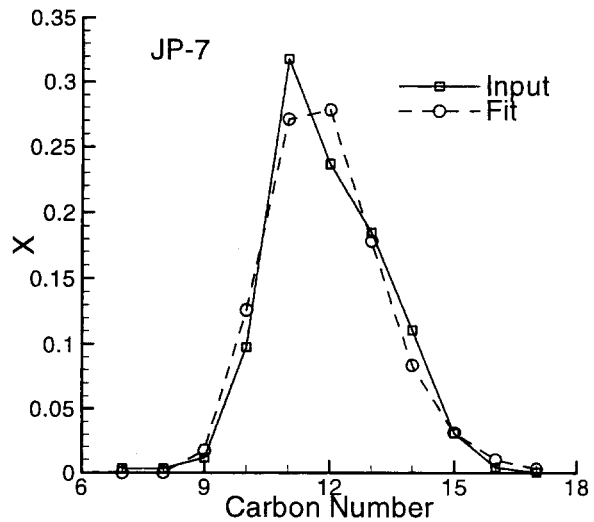


(d)

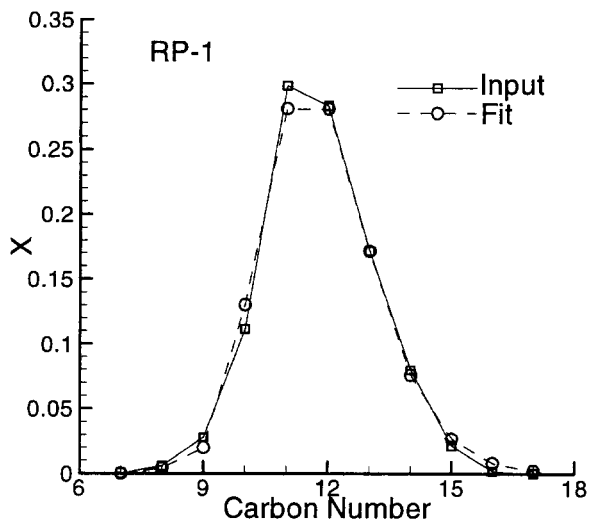
Figure 1.



(a)

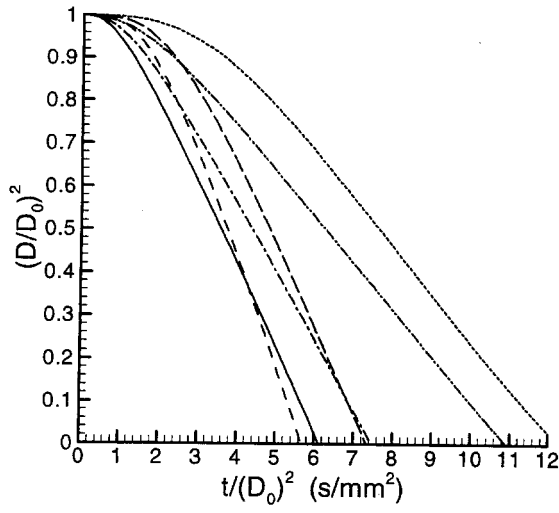


(b)

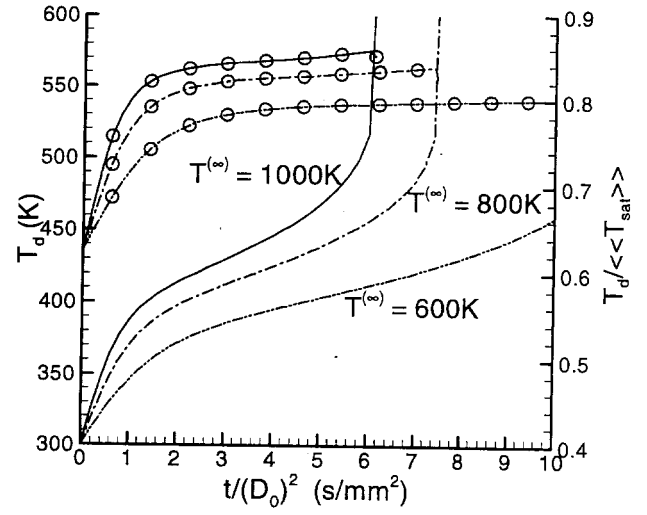


(c)

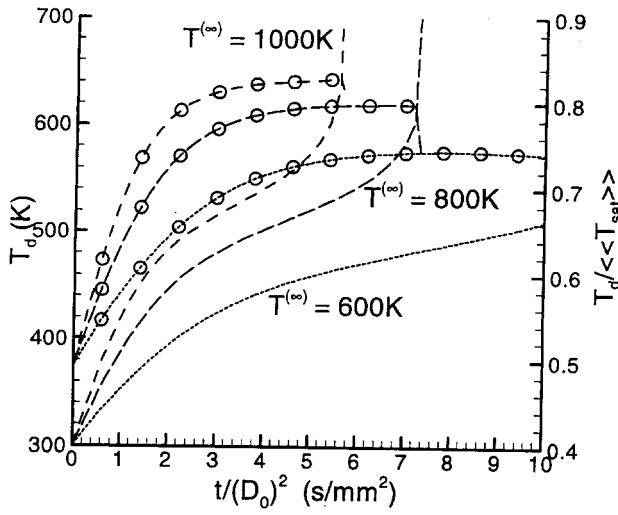
Figure 2.



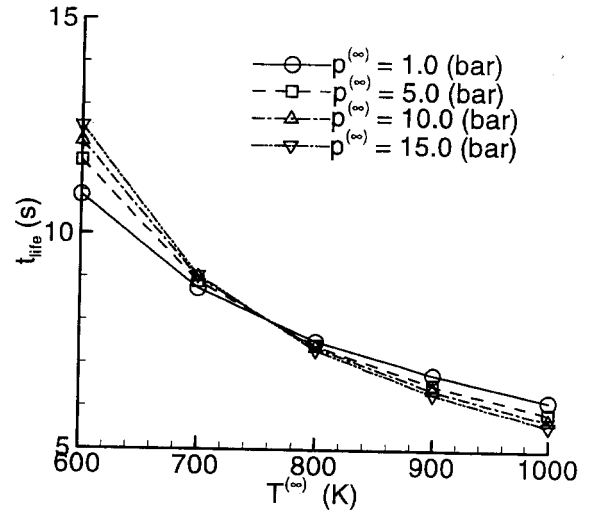
(a)



(b)

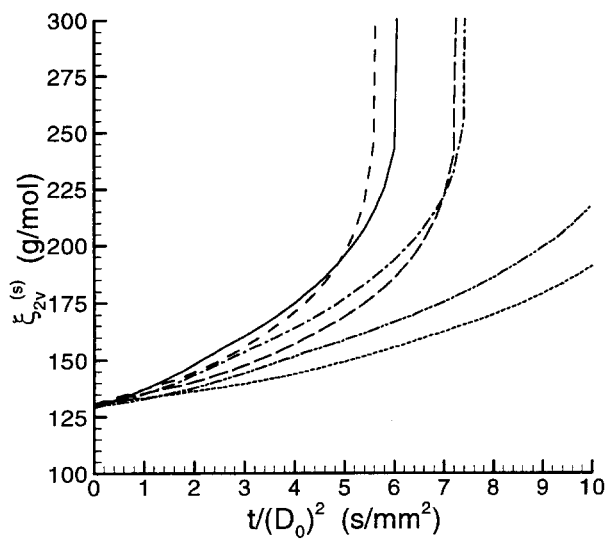


(c)

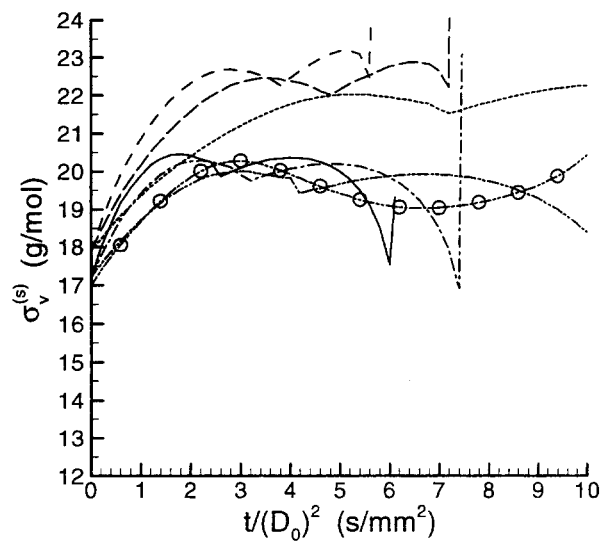


(d)

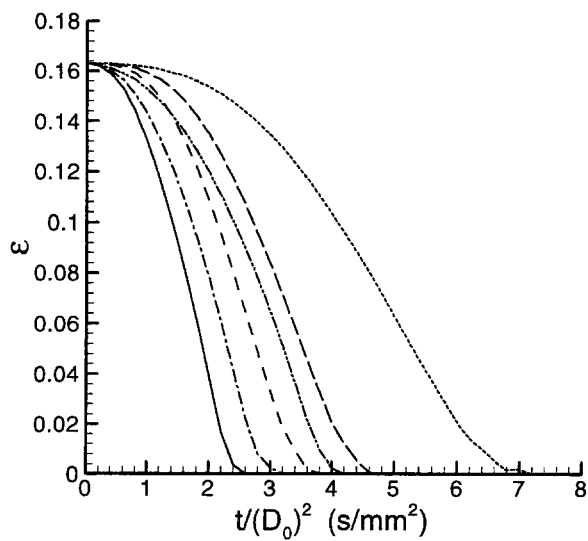
Figure 3.



(a)

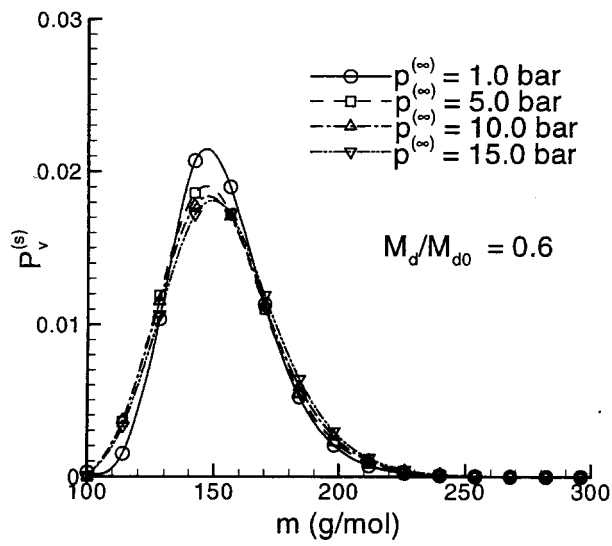


(b)

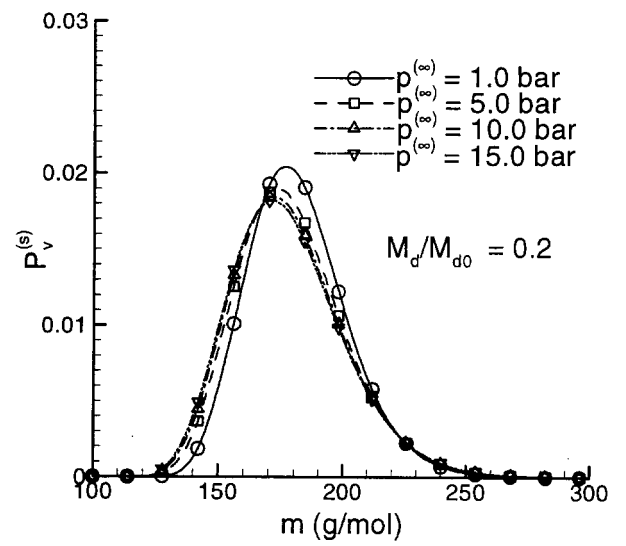


(c)

Figure 4.

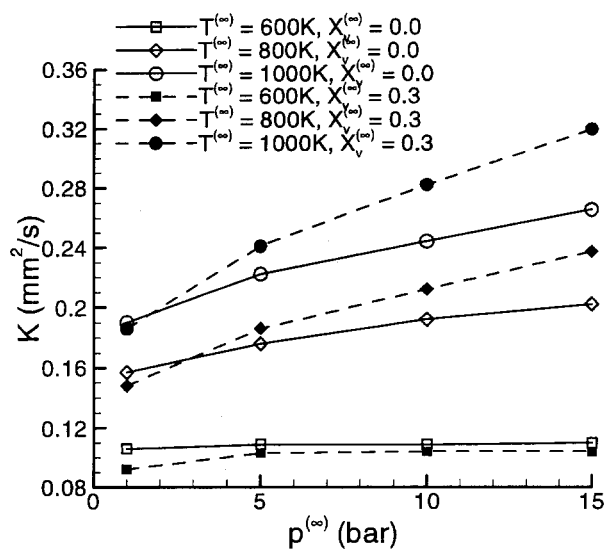


(a)

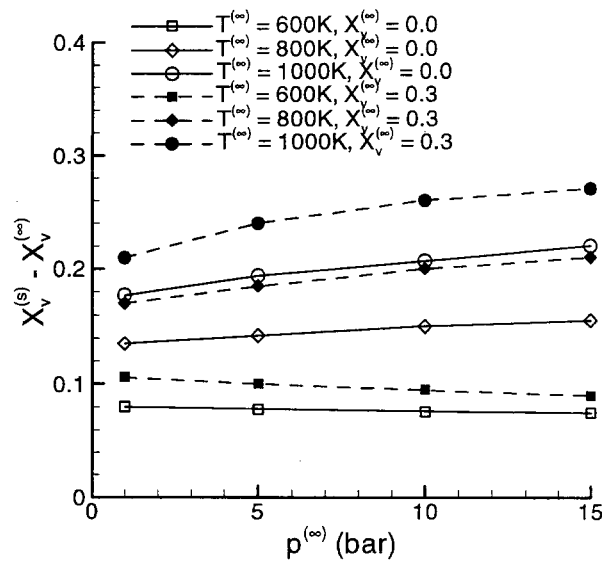


(b)

Figure 5.

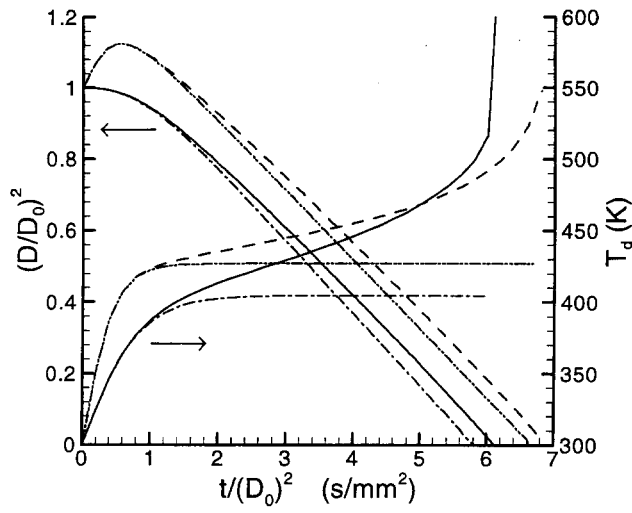


(a)

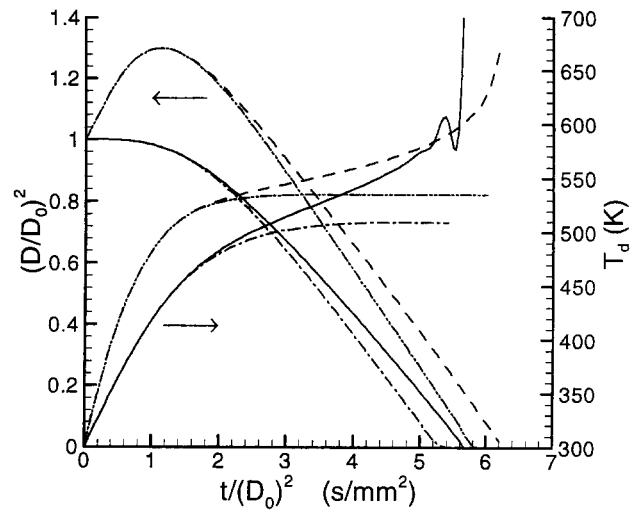


(b)

Figure 6.



(a)



(b)

Figure 7.

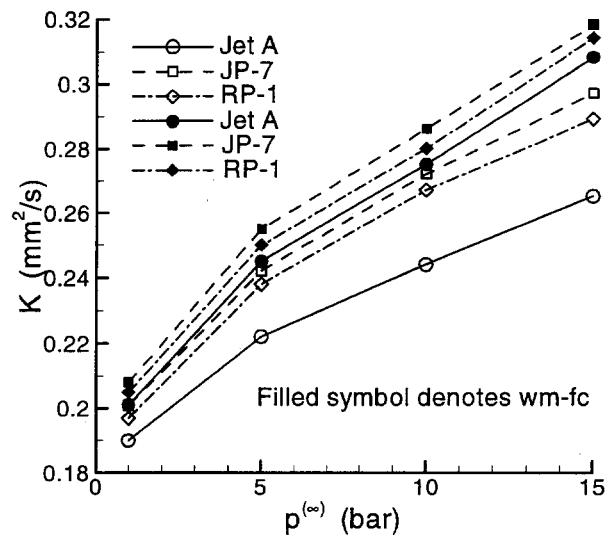
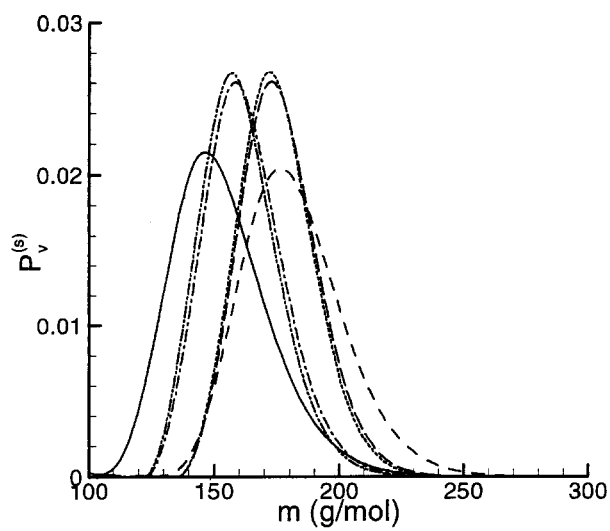
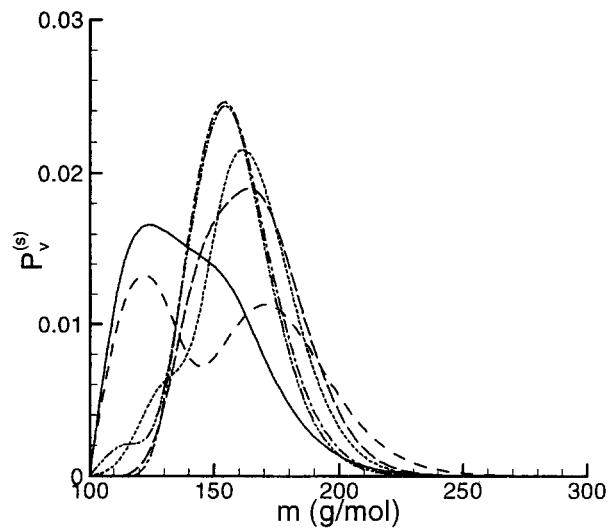


Figure 8.



(a)



(b)

Figure 9.